ELSEVIER

Physica C 222 (1994) 133–148

PHYSICA C

Nucleation and growth mechanisms of textured YBaCuO and the influence of Y_2BaCuO_5

N. Pellerin [a], P. Odier [a], P. Simon [a], D. Chateigner [b]

[a] *Centre de Recherches sur la Physique des Hautes Températures, CNRS, 45071 Orléans cedex 2, France*
[b] *Laboratoire de Cristallographie associé à l'université Joseph Fourier, CNRS, 38000 Grenoble cedex 09, France*

Received 15 November 1993; revised manuscript received 20 December 1993

Abstract

123 texturation has been achieved with success on Y_2O_3 without application of an external thermal gradient for the purpose of a better understanding of nucleation and growth mechanisms. We have studied the effects of thermal parameters such as the maximal applied temperature and crystallization speed. Their respective contributions to the peritectic recrystallization (211 consumption), and to the textured domain size have been made precise by using X-ray data and semi-quantitative analysis on the micrographs. The interface reaction between the Y_2O_3 substrate and 123 has been analyzed. The substrate promotes a seeded type growth of 123 owing to an interfacial 211 layer. The mechanism of crystallization has been analyzed in the light of existing theoretical models. Our data confirm a crystallization of 123 directly from a liquid as in a peritectic reaction where a major part is played by the yttrium diffusion in the liquid. Y atoms are supplied by the dissolution of 211 particles. According to Uhlmann–Chalmers–Jackson (UCJ) theory, coarsened 211 grains are trapped by the solidification front in contrast to particles smaller than a critical radius that are consumed in the peritectic reaction. (This process explains why such large 211 particles are obtained in MTG contrary to QMG or MPMG methods.) Moreover, EPR results show a preferential orientation of 211 inclusions according to the 123 matrix which could be favorable to flux pinning in the superconducting state. 211 oriented inclusions make possible, to some extent, heterogeneous nucleation at platelet–211 junctions. On the other hand, microstructural studies show that the liquid/solid interface is rather unstable being frequently cellular or dendritic, consistent with a model proposed by Alexander et al.

1. Introduction

The electric properties of the $YBa_2Cu_3O_{7-\delta}$ superconducting ceramics (we will in the following denote by *xyz* the $Y_xBa_yCu_zO_w$ composition) have been notably improved since 1988 by texturing in the presence of a liquid phase [1]. Texturation allows one to increase the grain connection [2], and so to raise the critical current densities J_c, especially under a magnetic field. Actually, the most general method for texturing is the melt textured growth (MTG) technique [3]. The best samples formed by this method achieve transport critical current densities J_c in the order of 5×10^4 A cm^{-2} at 77 K between 0 and 2 T (using pulsed currents) [4–7]. The MTG method uses peritectic melting of the 123 phase at $T_p = 1015$°C in air, giving rise to the Y_2BaCuO_5 phase (the so called green phase) plus a liquid ml having the approximate stoichiometry Y/Ba/Cu: 1/16/27 [8]:

$$123 \rightarrow 211 + L(ml)\,. \qquad (1)$$

A slow cooling step (at a rate close to 1°C/h) in a temperature range including T_p, and under a thermal

SSDI 0921-4534(93) E1062-B

gradient of 1 to 50°C/mm allows crystallization and texturation of 123 to occur. One obtains a textured matrix 123 containing 211 residual inclusions because of only partial peritectic recrystallization of 123 due to kinetic problems. However, up to now texturation concerns generally small samples (in the centimetric range).

The increase of J_c necessitates efficient vortex pinning and thus the presence of a large number of appropriate defects. Probably 211 inclusions act as pinning centers, but certainly indirectly [9,10]. A study of Murakami et al. shows J_c to be inversely proportional to the size of 211 grains [9]. Effectively, materials with a defect size in the order of magnitude of the coherence length, as in thin films, offer a very high J_c but exhibit also large flux creep. In these materials, defects are due to growth faults. In textured materials with large 211 particles ($d \geqslant 1$ μm), J_c is smaller, but flux motion is less affected by thermal activation.

Other methods derived from MTG have been developed with the purpose to control the 211 residual phase microstructure. The well known quench melt growth (QMG) [11] method allows one to obtain residual 211 particles with 1 to 5 μm size, while the melt powder melt growth (MPMG) technique, derived from QMG, leads to inclusions $\leqslant 1$ μm [11]. Even smaller 211 particles (0.5 μm), have been obtained by the powder melting process (PMP) starting from 211 and 011 mixed powders in the appropriate stoichiometry to get 123 [12].

Application of a thermal gradient G (°C/cm) allows one to increase the size of textured domains and subsequently to raise the J_c values [13,14]. For example, Pollard et al. [15] showed that a MTG experiment leads to a 500 μm 123 domain size without thermal gradient, while it reaches a few millimeters when $G = 10$°C/cm. Other authors have also tried to use different kinds of texturing means such as a magnetic field [16] or seed growth [17].

In directional crystallization, the growth rate R (cm/h) plays an essential role. The theory of constitutional supercooling developed for alloys [18] gives the conditions for establishing a stable planar solidification front, needed to obtain samples of high crystalline quality. This is mainly governed by the ratio G/R which must be sufficiently high to fulfill the inequality

$$G/R \geqslant -(mC_L/D_L)(1-k)/k\,,$$

where m is the liquidus slope (dT/dC_L), D_L the diffusion coefficient of the solute in the liquid phase, k the distribution coefficient at the interface and C_L the solute concentration in the liquid.

The product GR (°C/h) also plays an important role in the peritectic solidification. It is equivalent to a local cooling rate and controls the coexistence, the selection and the transformation of the phases [19]. Recent studies of Shiohara et al. by directional solidification (horizontal Bridgman configuration) show that the theory of constitutional supercooling can be applied to the peritectic recrystallization of high-T_c superconductor oxides [19,20].

If peritectic systems are very common in metallic alloys, very few fundamental research works have been performed on peritectic solidification of oxide systems, and especially on the precipitation of the secondary phase and its subsequent growth in relation to the dissolution of the primary phase. However, understanding this phenomenon is essential for the purpose of texturing large pieces of 123 ceramics with relatively high J_c and low flux creep. Peritectic crystallization is a complex mechanism and Kerr et al. [22] have introduced the distinction between peritectic reaction and peritectic transformation. The peritectic reaction described by $L+\beta \rightarrow \alpha$ is the formation of a secondary solid α by reaction of the primary phase β directly with the liquid at the peritectic temperature. Generally, this reaction does not go to completion because there is formation of a continuous layer of α which encloses each β particle, preventing further direct contact between liquid and β. The reaction can then continue thereafter only by long-range diffusion of the solute through the α-layer; this is termed a peritectic transformation. This is not usually isothermal since diffusion through the solid will limit the transformation rate. StJohn [23] showed that this first definition can in fact be discussed. In particular, he concludes that the peritectic reaction cannot occur at the peritectic temperature for thermodynamical reasons, and does not appear in most peritectic systems because crystallization of the peritectic phase must occur directly from the liquid. However, in peritectic systems where liquidus lines of the primary and secondary phases are close together, the liquid L may coexist with the peritectic

product α and with the primary solid β below T_p by undercooling. In this case a fast access to the primary phase is possible allowing the peritectic reaction to occur for continuous cooling, at moderate rates, below T_p. This peritectic reaction is rarely observed because it necessitates the dissolution of β in the undercooled liquid (Fig. 1) and the crystallization of α directly from the liquid. This particular case can be described, at T_R for example by the successive reactions (1a) and (1b) for the cooling of a melt of composition $C_{\alpha p}$ [23]:

$$\beta(C_\beta)+L(C_{L\alpha})\rightarrow L(C_{L\beta})\,, \qquad (1a)$$

$$L(C_{L\beta})\rightarrow \alpha(C_{\alpha 1})+L(C_{L\alpha})\,, \qquad (1b)$$

where $C_{L\alpha}$, C_β, $C_{L\beta}$, $C_{\alpha 1}$ and $C_{L\alpha}$ denote the concentrations defined in Fig. 1.

This theory is for example verified in Cu–Sn alloys [24] as well as in other usual compounds such as Al–Mn [25] and Pb–Bi [24], with evidence of primary phase dissolution.

Since 1992, different hypotheses have been proposed to discuss the mechanism of 123 peritectic recrystallization from 211+L(ml). Izumi et al. [21] have observed the radius of 211 particles in the 123 matrix, for samples obtained by directional solidification. It is almost constant and independent of the distance from the solid/liquid interface and of the growth rate R. They assume that a significant coarsening of the 211 particles occurs in the liquid by Ostwald ripening and that these grains are trapped in the growing crystals when they become larger than a critical radius, as described by Uhlmann–Chalmers–Jackson theory [26]. Then the solute (yttrium in particular) necessary to accomplish the peritectic solidification is supplied through the liquid according to the peritectic reaction mechanisms.

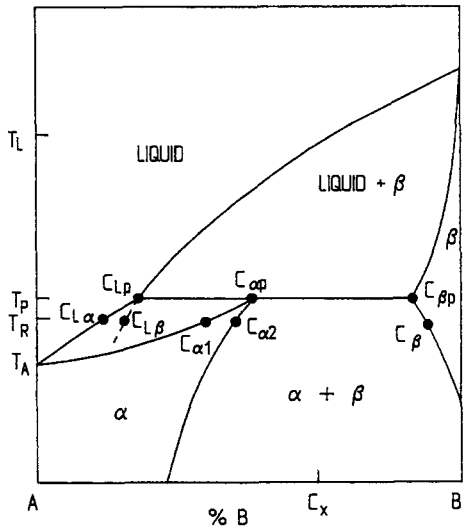

Fig. 1. Hypothetical phase diagram involving a primary phase β and a peritectic secondary phase α. It is associated with a case where the undercooled liquid β (composition $C_{L\beta}$) can coexist with the liquid α (composition $C_{L\alpha}$) and the solid β (composition C_β) at a temperature below T_p. The solid α (composition $C_{\alpha 1}$) is then directly solidified from the liquid. This is the so-called peritectic reaction according to StJohn [23].

In the same way, Bateman et al. [27] have argued that 123 texturation cannot be explained by considering that 123 is grown by nucleation on initial 211 particles and further being encapsulated. Effectively, one would then observe small randomly oriented grains of 123, perhaps with residual 211 particles at their center [18]. They also claim the inconsistently of this hypothesis from a kinetic point of view. Therefore 211 is not a preferential nucleation site for 123, contrary to the point of view of many authors [28,29]. Then it is obvious that peritectic recrystallization of 123 does not proceed according to the classical peritectic transformation. Bateman et al. suppose a dissolution of 211 and precipitation of 123 to take place from an undercooled liquid (undercooling of 30 to 100°C), according to the model proposed by StJohn [23]. Other authors have effectively observed peritectic growth of 123 below 1015°C [30], which presupposes the existence of undercooled liquids. To explain the 123 grain alignment, Bateman et al. assumed preferred nucleation sites of the peritectic product on heterogeneities and boundaries formed by sympathetic nucleation. This type of nucleation can be defined as the nucleation of a precipitated crystal, with a composition different from that of the matrix, at the interface boundary of another crystal of the same phase [31]. Sympathetic nucleation has often been observed in Fe-based, Cu-based or Ti-based alloys. A comparative theoretical study of the relative nucleation kinetics for homogeneous, grain-boundary and sympathetic nucleation demonstrates that the activation barriers associated with these processes become comparable when nucleation occurs on the terraces of the plate-shaped precipitate, and when the matrix/precipitate interface is replaced by a precipitate/precipitate bound-

ary having a relatively low energy. Small-angle precipitate/precipitate boundaries (few degrees) [31,32] are encountered in 123 textured matrix according to Bateman et al. [27] and sympathetic nucleation is assumed to take place. However, sympathetic nucleation refers to multiphase compounds at equilibrium, which is not strictly the case here.

Finally, Alexander et al. [33] have put forward another hypothesis on the growth process. They have observed the presence of crystallized phases between the boundaries of stacking sheets. On the other hand, they observe a very small crystallographic misorientation between the sides of boundaries within a domain, which we confirmed in another study [34]. This is considered as a proof that a crystalline continuity exists in a domain therefore identified as a single crystal. They conclude that 211 particles contribute to the boundary-formation process because the crystal must bypass these particles during progression of the solidification front. These boundaries are filled with products rejected by the liquid phase during 123 bidimensional cellular solidification.

The substrate is an important aspect of the texturation and very few papers have been published concerning nonpolluting substrates such as Y_2O_3 [35] or Y_2BaCuO_5 [36]. The purpose of this article is to demonstrate that it is possible to texture on relatively large dimensions, without external driving forces, by using a polycrystalline Y_2O_3 substrate. This oxide is very interesting because it does not pollute the superconducting phase. We therefore report on texturing experiments on this substrate performed without external thermal gradient or magnetic field. This may be a simplification necessary for a better understanding of the mechanisms. We have studied the effects of thermal parameters such as the maximal temperature reached and the crystallization rate. From microstructural and chemical studies we try to differentiate their respective contributions on the maximal domain size and on the peritectic recombination efficiency. This discussion enables one to separate the contribution to the process of this particular substrate. Finally, we show that the characterization of 211 residual particles gives interesting information concerning the crystallization process. Comparison of our results with those of other authors helps to discuss the models proposed in the literature.

2. Experimental procedure

$YBa_2Cu_3O_{7-\delta}$ powders are prepared from Rhône-Poulenc powders (RP 43, SU 86 or RF 183) and Alcatel-Alsthom Recherche (centre de Marcoussis, France) precursors, by firing in oxygen at an increasing temperature with intermediate grinding. The presence of unreacted phases is checked by careful X-ray diffraction (XRD) characterizations (Philips diffractometer with Ni filtered Cu Kα radiation). When a single phase is obtained, the powder is isostatically pressed (at 250 MPa) in a cylindrical shape ($\varnothing = 4$mm, $l = 15$ mm), and sintered at 900°C in O_2. The ceramic is then flattened on one side and positioned on the substrate. This support is an optically polished high-temperature sintered disk of Y_2O_3 (95% d_{th}), prepared from pure Y_2O_3 powders (3N, Rhône-Poulenc).

The sample and its substrate are placed in an horizontal furnace in such a way that the axis of the sample is collinear with that of the furnace. The longitudinal thermal gradient along the sample is negligible in this portion of the furnace, and the radial gradient is estimated to be smaller than 1°C/cm. The heat treatment is made according to the profile of Fig. 2 (top). The sample and its substrate are brought from room temperature to an elevated temperature denoted T_{max} ($1030 \leqslant T_{max}$ (°C) $\leqslant 1170$) in 3 h. This temperature is maintained during t_M (0–5 min or 1 h); the sample is then cooled at a rate C_d (0 to 200°C/h) to the temperature T_1 ($1005 < T_1$ (°C) < 1090). This first treatment allows the peritectic decomposition of 123 in 211 plus liquid to occur. Next, a slow cooling step at the rate C_r (0 to 5°C/h) is applied down to T_2 ($980 < T_2$ (°) < 1020) to perform the peritectic recrystallization of 123. A post-reoxygenation annealing under pure oxygen flow is made (see Fig. 2 (bottom)).

The textured samples are then analyzed by several techniques. SEM (Cambridge stereoscan 100) is used for morphological characterizations. It is coupled with an EDS analysis. The use of standard spectra of pure 123, 211, 011 and 001 phases allows one to identify unambiguously the implied phases. Observations are made on polished and chemically etched cross-sections with an aqueous solution of 2%vol. acetic acid). Observations of the Y_2O_3/123 interface are also made on cross-sections perpendicular to the substrate sur-

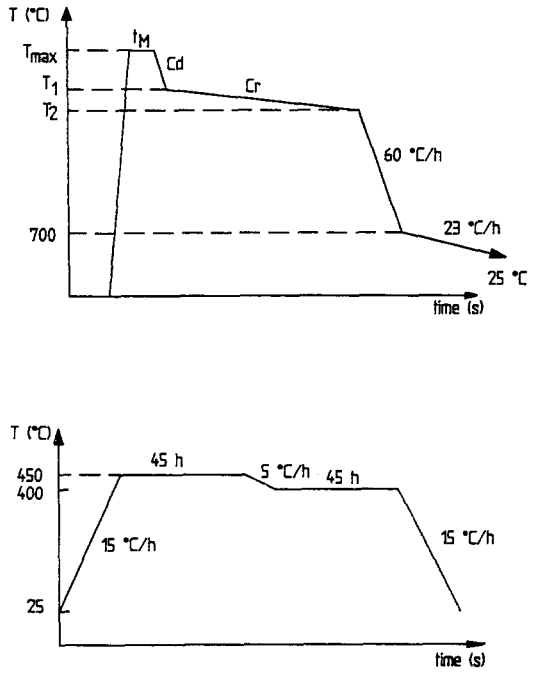

Fig. 2. Temperature profile for the 123 texturation (top) and reoxygenation procedure (bottom).

face. These have been completed by quantitative analysis with an electron microprobe (Camebax-microbeam) using wavelength dispersive analysis (WDS). The spectrometer works under 15 kV with a current beam of 12 nA and a spot size of 1 μm. Calibrations are made on pure Cu, $BaSO_4$ and Y_2O_3 by using PET crystal analysor for Ba Lα, LiF for Cu Kα and TAP for Y Lα. Oxygen was not detected in this study; its contribution was estimated by assuming a normal oxidation state of the elements. We used ZAF corrections to obtain Y, Ba and Cu atomic fractions measured each micrometer. The measurements on porous areas are not taken into account.

Quantitative information on the microstructure of textured 123 is needed to determine the role of the various thermal parameters. These quantities should be only used for comparing samples and not as absolute data. From micrographs obtained on several sections parallel or perpendicular to the substrate, we have roughly estimated the volume of the largest domain of each sample: it is denoted V_{max}. A domain is defined [37] as a zone with weakly misoriented (few degrees) grains separated by boundaries clearly visible in Fig. 3. Domains are easily visible in an optical

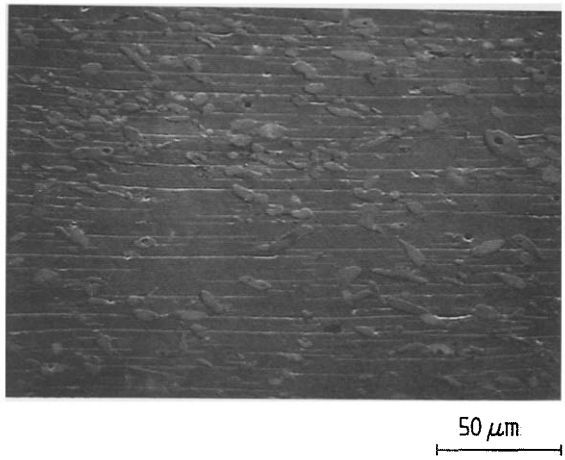

Fig. 3. Typical texture of 123 (sample R102, Table 1). The sample has only one large single domain.

microscope. We have also estimated the mean size l_m and the surface density d_s of residual 211 grains from SEM photos. They appear as lengthened particles with a bright contrast. The quantity l_m is approximated by the mean value of their individual largest dimension over one hundred particles localized on a surface of area S. Assimilating the 211 particles to rectangulars of surface $s = l_m \times l_m/2$, then the surface density d_s is simply deduced from

$$d_s = 100\, s/S = 50 l_m^2/S\,.$$

Accounting for measuring errors gives a 6% relative error for S, 15% for l_m, and 30% for d_s, which is large, but allows for comparison between samples.

Whereas d_s gives local information on the 211 surface density, we have searched to obtain a macroscopic order of magnitude for the 211 volume fraction relative to 123. To do so, we used representative parts of the samples, finely ground and probed by X-ray diffraction. After estimating the base line, we evaluate the intensity I of the (hkl) lines (110) and (013) for 123, and (140), (002), (211) and (131) for 211 phase by their amplitude. This enables one to calculate $I_{123} = I(110) + I(013)$, and $I_{211} = I(140) + I(002) + I(211) + I(131)$. These lines are intense and poorly affected by the degree of powder orientation; this allows one to reasonably assume the ratio $r_i = I_{211}/(I_{123} + I_{211})$ to be proportional to the relative volume fraction of 211 phase in the sample. Considering the different sources of error (sample homogeneity, degree of powder oxygenation ...), we

can estimate the relative error on r_i to be in the range of 20%.

Conventional X-ray diffraction and XRD pole figures [38] were also used to analyze the texture. The pole figures are obtained by using the Schulz reflection technique. The intensity distribution is measured by the appropriate φ and χ ($0<\varphi<360°$ and $0<\chi<72°$) scans. The analyzed area is in the order of 1 mm^2 ($\approx$ 10 μm in depth). After an appropriate treatment of the data, the pole figures are plotted on a polar stereographic projection.

Additional EPR studies were made to study any orientational relationship between the 211 phase and the 123. The EPR spectra have been recorded at room temperature in air, on a X-band and on a Q-band spectrometer, respectively, for $\nu \approx 9.7$ GHz and $\nu \approx 34.2$ GHz.

To analyze the chemical reactions between the liquid ml and the substrate, we have made thermal analysis by DSC (Setaram 1500°C) on a mixed powder composed with 60 mg of ml (prepared by the sol gel technique [39]), and 240 mg of Y_2O_3 (3N Rhône-Poulenc). The resulting powders were also analyzed by XRD.

Finally, AC magnetic susceptibility and magnetization measurements were made to check the superconducting properties.

3. Results

We have brought together in this section the experimental facts observed. The discussion is focussed on extrinsic factors concerning texturation caused by the particular choice of yttrium oxide substrate and the absence of imposed thermal gradients. Section 4 concerns more intrinsic aspects of texturation.

3.1. Influence of the thermal schedule

Experiments have been performed to delimit the influence of several parameters, i.e., T_{max}, t_M and C_r (see fig. 2), on the texturation performed on Y_2O_3 and without thermal gradient. The samples may be characterized by four parameters defined in section 2: V_{max}, d, I_m and r_i. In addition, the expected correlation between d_s and r_i allows one to appreciate the homogeneity of the 211 repartition in the sample. The role of the cooling rate C_r is discussed first, but before going into more details, one should recall some general observations.

After texturing, the cylindrical shape of the samples is preserved. Generally the samples are dense and homogeneous, but metallographic observations reveal the presence of some heterogeneous zones, often localized at one end and/or at the periphery of the sample. These areas are disordered, and copper-rich with many accumulated 211 particles. A representative example of such a case is shown in Fig. 4. The samples stick on the substrate which becomes black with green zones because of some reacted liquid evacuated from the sample by wetting. This will be developed in section 3.2.

3.1.1. Slow cooling rate, i.e. $C_r = 1°C/h$; the role of T_{max} and t_M

In all cases discussed here, the starting temperature of the cooling sequence T_i is 1030°C, that is 15°C above the peritectic temperature, and the cooling rate C_r is 1°C/h.

Data characterizing the textures versus T_{max} and t_M are reported in Tables 1 and 2. From Table 1, it is clear that V_{max} increases with T_{max} up to an optimal temperature depending of the time spent at the high-temperature plateau. At first sight, the increase (not shown here) is linear with T_{max} for T_{max} below 1140°C. In our particular case V_{max} reaches a maxi-

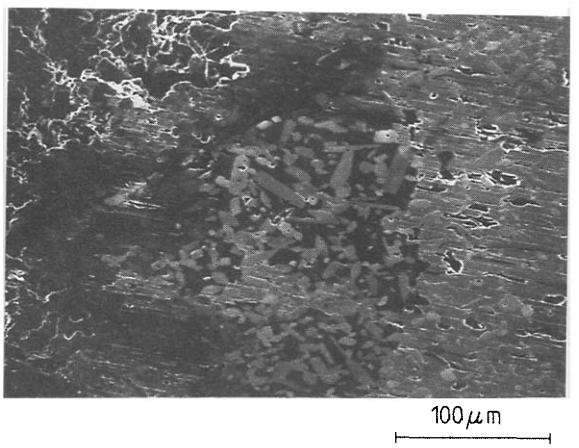

Fig. 4. An example of large heterogeneities frequently observed at the perifery or at the extremities of textured samples. One sees the texture at the right hand side, large black copper-rich inclusions containing many 211 particles and porosities at the left-hand side (sample R101, Table 2).

Table 1
Influence of T_{max} and T_M on texture formation as quantified by l_m, d_s, r_i and V_{max} (see text for the definition of these quantities). Here $C_r = 1\,°C/h$, $T_1 = 1030\,°C$, $T_2 = 980\,°C$ and $C_d = 180\,°C/h$

Sample	t_M (min)	T_{max} (°C)	l_m (μm)	d_s (%)	r_i	V_{max} (mm^3)
R97	0	1030	7	29	0.3	2.4
R141	5	1030	6	20	0.23	30
R142		1060	6	18	0.18	65
R101		1090	7	22	0.28	90
R143		1110	6	23	0.27	90
R102		1140	7	18	0.31	130
R123		1170	6	24	0.39	65
R113	60	1030	6	25	0.33	1.5
R100		1090	7	16		65
R118		1140	7	12	0.34	0.3

Table 2
Influence of the cooling rate C_r on the texture for $1030 < T_{max}$ (°C) < 1170, $0 < t_M$ (min) < 5, $T_1 = 1030$ or $1040\,°C$, $T_2 = 980\,°C$ and $0 \leqslant C_d$ (°C/h) $\leqslant 222$. In bold are reproduced results of samples of Table 1 obtained for the same T_{max}

sample	C_r (°C/h)	T_{max} (°C)	t_M (min)	C_d (°C/h)	T_1 (°C)	l_m (μm)	d_s (%)	r_i	V_{max} (mm^3)
R105	4	1030	0	0	1030	6	6	0.17	0.1
R97	**1**			**180**		**7**	**29**	**0.3**	**2.4**
R107	2	1090	0	180	1030	7	25	0.26	78
R101	**1**		**5**			7	**22**	0.28	**90**
R121	3	1140	5	180	1030	6	9	0.22	0.5
R102	1					7	18	**0.31**	**130**
R125	5	1170	5	222	1040	6	13	–	3
R123	**1**			**180**	**1030**	**6**	**24**	**0.39**	**65**

mum size for $T_{max} = 1140\,°C$ and for $t_M = 5$ min, the largest domain reaches 130 mm^3 ($10 \times 3.6 \times 3.6$ mm^3). One can draw an experimental efficient texturing range (T_{max}, t_M) as depicted schematically in Fig. 5. More research is in progress to make precise its limits, but it appears that the best compromise is realized at intermediate temperatures ($1070 \leqslant T_{max}$ (°C) < 1170) for a holding time between 0 and 30 min.

This compromise is found better evidence for by analyzing the correlation between d_s and r_i. The quantity d_s is associated with the amount of 211 phase remaining in the texture while r_i concerns its volume fraction. Unreacted 211 is due either to slow kinetics of the peritectic reaction or to shifts in the liquid stoichiometry due to possible reactions with the substrate. For homogeneously distributed 211 particles, one expects d_s to be proportional to $r_i^{2/3}$ because d_s is equivalent to an area (l^2) and r_i to a volume (l^3). This is verified ($d_s = a r_i^{2/3}$ ($a \sim 2.6$)), except for the samples R105, R121 and R118. The last two are high-temperature treated samples emphasizing the role of chemical interactions with the Y_2O_3 substrate. This is discussed in more details in section 3.2. On the contrary, sample R105 is processed at low T where still rather strong heterogeneities had developed. This is an indication that some dwell time is needed to get a homogeneous distribution of 211 solid phase within the liquid m1. Of course the higher the T, the smaller this time should be.

Because of the errors on d_s we can conclude from Tables 1 and 2 that d_s and l_m are rather insensitive to the operating conditions. However, a small decrease of d_s upon increasing T_{max} is noted for large t_M (in the range of 1 h). This indicates a more efficient recombination probably due to finer 211 particles. This

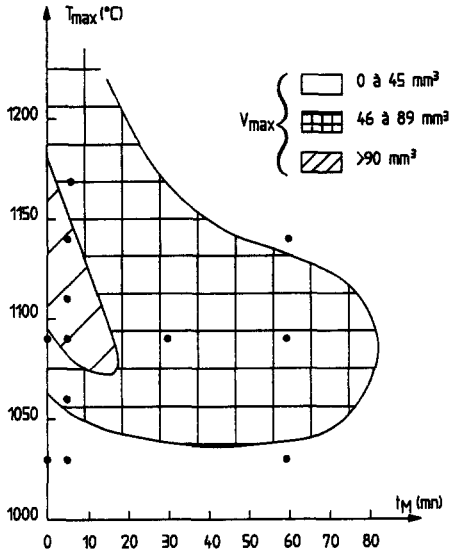

Fig. 5. A 2D schematic representation of $V_{max}=f(T_{max}, t_M)$. Lines are only guides for the eyes, V_{max} is the volume of the largest domain.

will be commented on according to the mechanisms of peritectic recrystallization in the discussion (section 4). Note that the values d_s and r_i are generally relatively large; effectively, the peritectic recrystallization of 123 is always incomplete. Finally l_m is remarkably constant between 5.7 (± 0.5) and 7.2 μm (± 0.5) for $1030 \leqslant T_{max}$ (°C) $\leqslant 1170$ and $0 \leqslant t_M$ (min) $\leqslant 60$.

3.1.2. Cooling rate $C_r \geqslant 2$° C/h

The cooling rate is an important aspect of the crystallization process because it represents the local transformation speed as defined by GR. It is then expected to have an influence on the solid/liquid interface stability. As an example, Fig. 6 shows a typical microstructure of samples processed at too fast cooling rates. Texture is still observed but on a local scale. No long-scale stacking seems possible above 4°C/h. Table 2 and Fig. 7(a) compile the representative set of our data in a useful way for optimizing V_{max}. For a given T_{max}, the largest domain size decreases versus C_r very rapidly (Table 2) indicating how critical should be the local equilibrium on long-distance development of ordered microstructures. This can be also appreciated in Fig. 7(b) where V_{max} has been plotted versus C_r for various T_{max}'s. Only a limited amount of data is available but it is observed that the

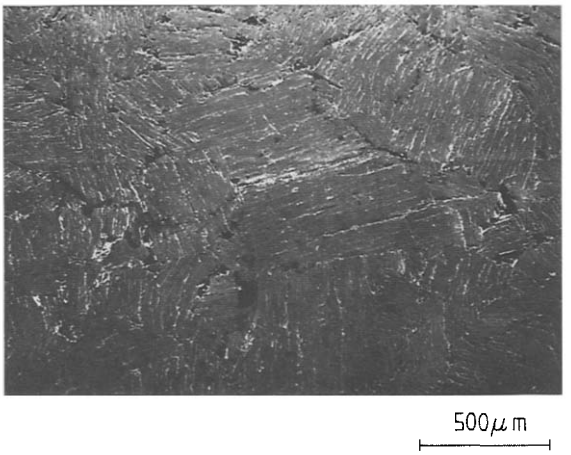

Fig. 6. A sample processed at a high cooling rate, i.e. $C_r=4$°C/h (sample R105, see Table 2). Textured domains are already formed but on a short scale.

development of a significant single domain is impossible above a critical C_r.

Another interesting feature is the fact that d_s and r_i both decrease upon decreasing the cooling rate. As an example, sample R105, to which a fast cooling rate $C_r=4$°C/h was imposed just after reaching T_{max}, has the smallest residual 211 content of the series because a smaller compositional shift competes with the peritectic recombination process. The substrate is responsible for such effects as will be now discussed.

3.2. Y_2O_3/123 interaction

The substrate is one of the key factors for texturing. Regnier et al. have shown for example that texturation by creep-sintering is possible on silver foils and not on pure gold [40]. We previously showed that, in the absence of a thermal gradient, no texturation was possible on Al_2O_3, only millimetric textured grains were achieved on single-crystalline MgO while textured grains 10 or 100 times larger were possibly reached on Y_2O_3 [41]. A careful analysis of the interface is then essential. SEM observations and EDS analysis on transverse sections across textured samples show a 211 interphase layer, about 200 μm thick, oriented in the same way as the 123 textured matrix, see Fig. 8(a). Quantitative chemical analysis by using the electron microprobe (WDS) allows one to confirm this. Figure 8(b) reports the chemical profile across a similar (but thinner) interphase as that shown in Fig. 8(a). Evidence is found for a well de-

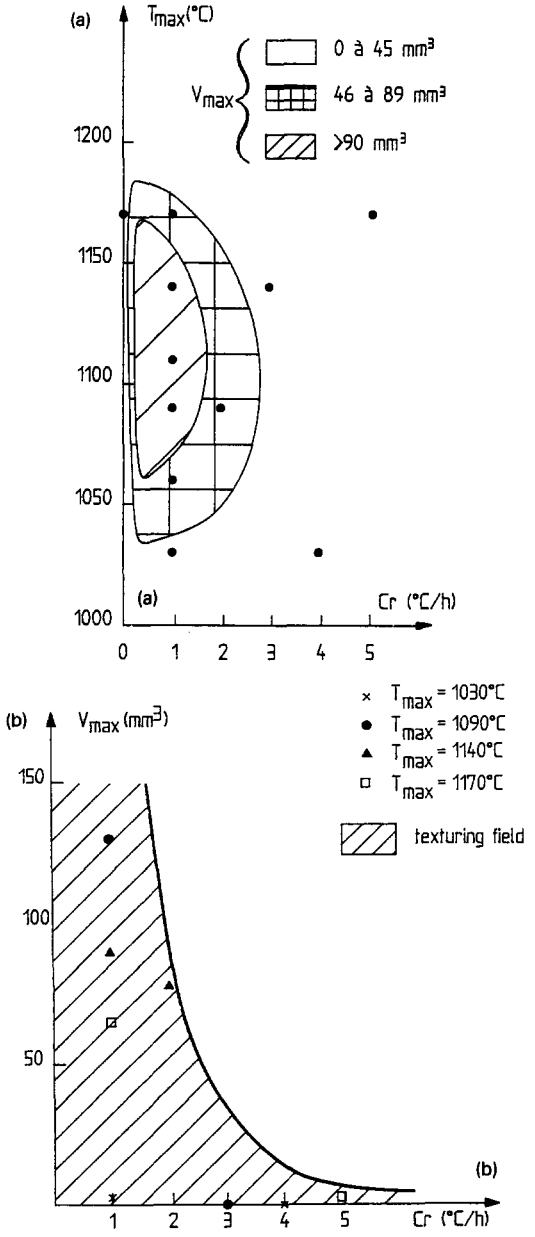

Fig. 7. (a) A 2D schematic representation of $V_{max}=f(T_{max}, C_r)$ compiled from our data (it includes variable conditions on T_1, T_2, $0 \leqslant t_M$ (min) $\leqslant 5$ and C_d). (b) V_{max} vs. C_r, for different T_{max}'s (and identical $T_1=1030°C$, $T_2=980°C$ and $C_d=180°C/h$). No texturation seems possible outside the hatched field.

fined zone (50 μm) composed of 211 phase; it is followed by an area composed exclusively of CuO+211, and 123 is detected on top. Similar findings were observed in a previous study of the chemical interaction of BaO/CuO melt on Y_2O_3 [42]. In this latter case, the liquid composition was close to 7BaO–18CuO (nearly the binary eutectic composition) and the results were almost identical except that the 211 phase was formed below 1000°C, i.e. at 940°C, corresponding to the peritectic temperature T_p.

Thermal analysis on powdered mixtures of ml and Y_2O_3 in the molar ratio $ml/Y_2O_3=1.2\times10^{-2}$ allows one to analyze more carefully the chemical reactions occurring between the liquid ml and the substrate. The DSC analysis, see Fig. 8(c) reveals the presence of a single endothermic peak at about 1050°C (onset at 1040°C). According to XRD analysis, the resulting sample is mainly composed of Y_2O_3, 211, and a small quantity of $Y_2Cu_2O_5$. This onset temperature corresponds with the observations of a texturing threshold at $T_{max}>1050°C$ (Figs. 5(b) and 7(a)) which then proves the need of a 211 layer at the interface for texturing on Y_2O_3. This is probably an essential step in the absence of a thermal gradient. Obviously no such layer could be formed on Al_2O_3 and MgO substrates [41]. This is a clear indication that 211 acts as a seed in the growth process. Certainly important is the fact that the 211 layer is apparently textured. The orientational relationship between Y_2O_3 or 211 precipitates and 123 have often been noted, in particular during crystallization of thin films [43,44,36]. However, our observations are a little surprising because our Y_2O_3 substrate is polycrystalline and the origin of the 211 orientation is not known. More work is presently under way on this aspect.

If Y_2O_3 has a beneficial influence on texturing in the absence of any imposed thermal gradient, it has a detrimental effect as the chemical interaction with the substrate may shift the overall composition. Clearly when the sample is subjected to a too high T_{max} or if a too long time (t_M) is spent at T_{max}, then part of the sample becomes green and porous. The removal of a significant amount of liquid during the process is responsible for this trouble. The liquid wets and reacts with the substrate which may be entirely green at the end of the process. Fig. 9 is an example of such a case where the right-hand side of the photo gives evidence of a porous zone exclusively composed of 211. Obviously the growth of the texture has been stopped on this zone due to the absence of a feeding liquid. Note that the physical characteristics of the remaining liquid do not permit one to fill back such an emptied

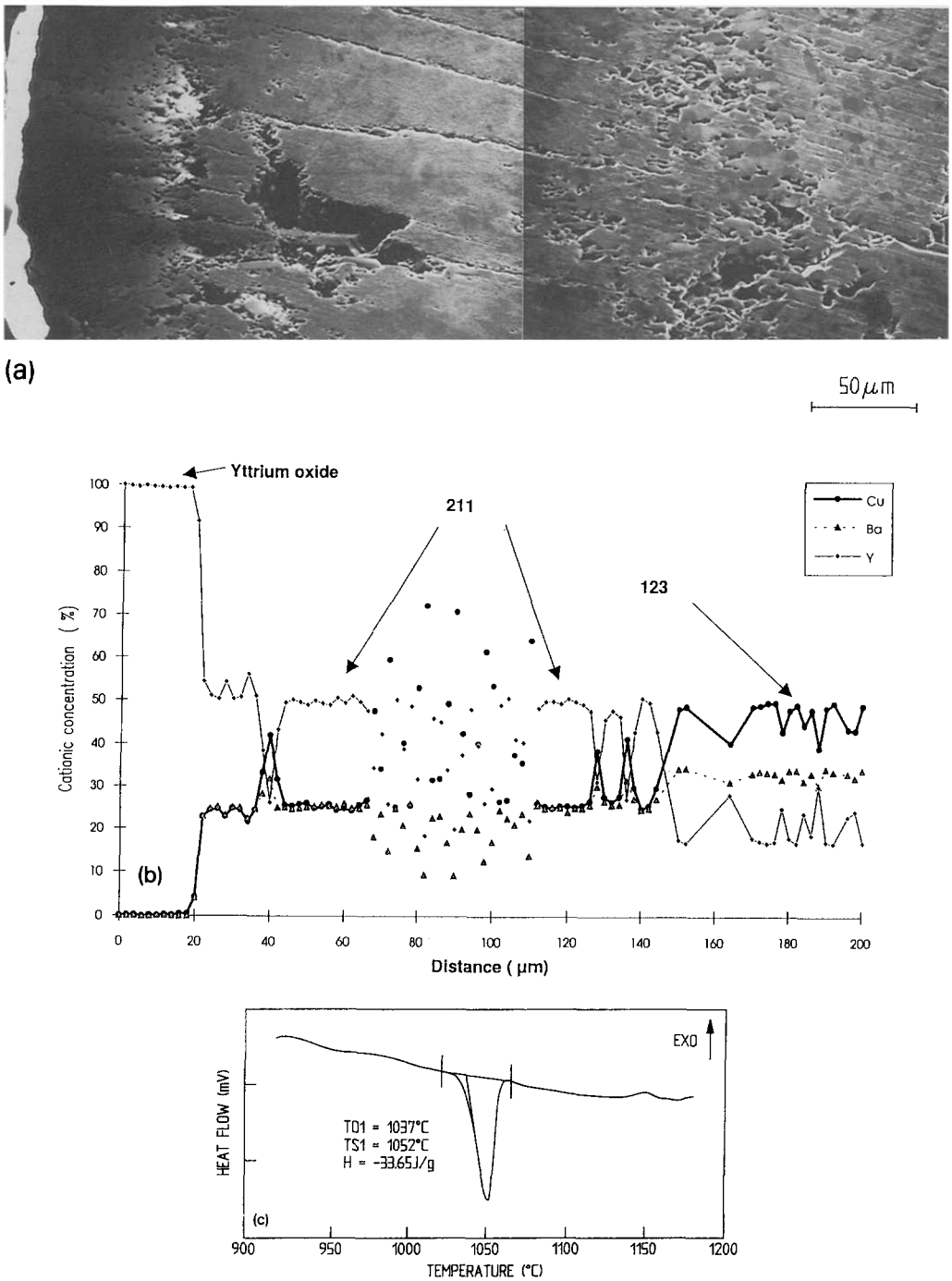

Fig. 8. (a) Cross-section of a textured sample (right part) on an Y_2O_3 substrate. (b) Chemical analysis profile (by electron microprobe in WDS) across the substrate and the textured 123 on top of it. (c) DSC analysis of a mixture ml/Y_2O_3 (molar ratio 1.2×10^{-2}), performed under air (ml refers to the liquid issued from the peritectic melting of 123, see text). This thermogram clearly shows the occurrence of a chemical reaction at 1040°C.

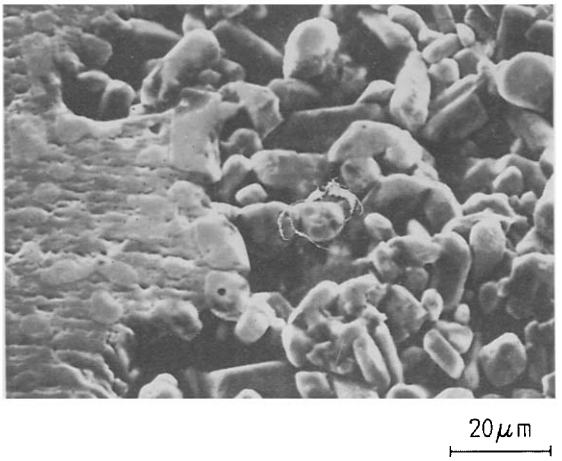

Fig. 9. A typical example where too much liquid has been removed from the sample by reactive wetting on the substrate, due to a too long holding time at T_{max} (sample R113, see Table 1). The grains on the right-hand side are 211 grains with almost no residual trapped liquid.

zone. On the other hand the aspect of the right-hand part of the photo of Fig. 9 gives a view of what would have been obtained if the liquid part of a melted sample of 123 would have been removed. It reveals the skeleton built by the 211 particles which inhibits significant deformation of the solid in its molten state [45].

Therefore, nucleation, growth and subsequent orientation of 211 is favored on Y_2O_3 in the presence of such a liquid as ml. It is apparently transmitted to 123 during its peritectic recrystallization, as the $(ab)_{123}$ planes appear to grow according to the texture developed at the 211 interphase. So, in the absence of any imposed thermal gradient, Y_2O_3 seems to drive the 123 texturation thanks to 211 growth which acts as a seed for 123 texturation.

3.3. Texture characterization

The analysis of the texture by XRD pole figures has been performed on two perpendicular surface. It shows that the texturation concerns the (ab) planes and is not limited to the surface of the specimen. Figure 10 shows several (hkl) poles for one typical sample (a part of sample R102, see Table 1). Areas delimiting the various intensity ranges are represented in the (χ, φ) plane. The $(00l)$ pole shape defines the

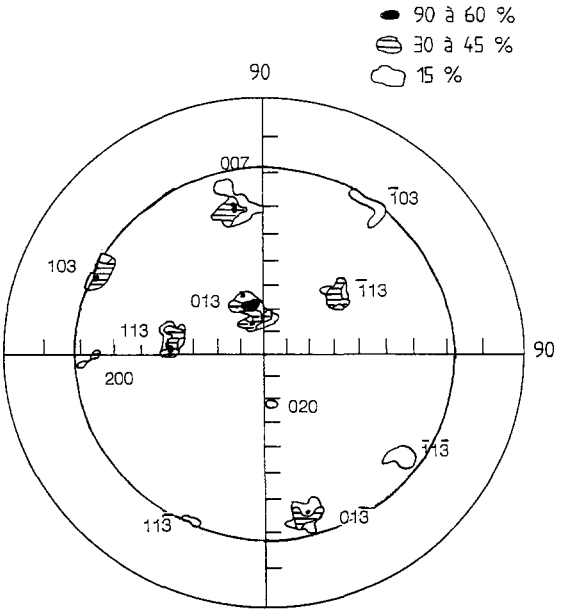

Fig. 10. XRD pole figure of a small piece (13 mm^2) of a large single domain (sample R102) processed on Y_2O_3. The plot is made in the (χ, φ) plane. The sample plane is the projection plane of the pole figures. The outline delimits areas covered by a given percentage of the maximal intensity.

degree of c-axis alignment. Its actual position proves that the [001] direction is at about 60° of the normal to the surface of the sample. The (hkl) pole figures give information on the in-plane texture. In addition it can be used to evaluate the angular dispersion of the platelets considering the solid angle containing the (hkl) poles. Taking into account only the crystals contributing to more than 50% of the maximal intensity, their angular dispersions are limited to less than 5° for all the crystalline directions ascertaining the rather small mosaïcity of this sample. We can conclude that this method of texturation provides a bulk texture of good quality.

Our textured samples present some macroscopic cracks between the sheets. Their orientation can be estimated from the XRD pole figures, they are coplanar with (ab) plans, and follow the cleavage (001) plane although substantial deviation may be noted on a local scale. The presence of cracks in our samples is difficult to control; they are occasionally formed even under slow cooling below 700°C (Fig. 2(a)). Probably the tetragonal-to-orthorhombic phase transformation, the residual stresses between 211 and 123 and also the differences in thermal-expansion coeffi-

cients between 123 and Y_2O_3 substrate have to be considered together.

We have also explored the possibility of an orientation of the 211 residual phase according to 123. Comparing XRD intensities of 211 powder and of 211 in textured samples tends to prove that 211 is also preferentially oriented. This has been made precise with an EPR study thanks to the absence of any detectable 123 EPR signal, an absence not yet understood [46,47]. Conversely, owing to the presence of localized Cu^{2+} of spin $\frac{1}{2}$ in the 211 compound, this phase displays a strong EPR signal. The local environment of 211 is orthorhombic, and in a single crystal, the principal axes of the $\boldsymbol{g}$ tensor coincide with the crystallographic axis: g_x with $\boldsymbol{a}$, g_y with $\boldsymbol{c}$ and g_z with $\boldsymbol{b}$ ($\boldsymbol{a}=0.5658$ nm, $\boldsymbol{b}=0.7132$ nm, $\boldsymbol{c}=1.2181$ nm) [48]. The splitting g_x-g_y being small, we denoted g_l for the mean arithmetic value of g_x and g_y, while $g_\parallel$ corresponds to g_z. Several textured single-domain samples have been analyzed by EPR in a configuration allowing for an axial rotation of the sample. Fig. 11 shows measurements performed with the rotation axis perpendicular to $\boldsymbol{c}_{123}$. An analysis of the different angles ($\boldsymbol{H}$, $\boldsymbol{c}_{123}$) shows a maximum of the line associated with $g_\parallel$ when the magnetic field is perpendicular to $\boldsymbol{c}_{123}$. This is a proof that green residual particles are preferentially oriented with regard to the

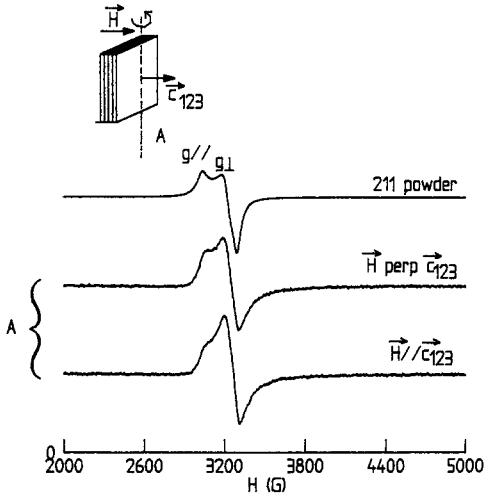

Fig. 11. EPR of a 123 textured sample. The copper signal is that of 211 residual inclusions. It is compared to that of the pure 211 powder. The sample can be rotated with respect to the vertical axis. The signal (curves A) is anisotropic due to a preferential orientation of the 211 particles inside the texture.

$YBa_2Cu_3O_{7-\delta}$ matrix: the $\boldsymbol{b}_{211}$-axis is then contained in the $YBa_2Cu_3O_{7-\delta}$ (ab) planes. A more precise study has been made in the Q-band. At first observation, it seems that the $\boldsymbol{c}_{211}$- and $\boldsymbol{a}_{211}$-axes present no preferential orientation with 123. TEM observations of the 123/211 interfaces on similar samples [49], and results reported from the literature [50] are consistent with this EPR study.

3.4. Magnetic measurements

The textured samples have been characterized in AC susceptibility proving high-superconducting properties. The best one displays a perfect diamagnetic behavior below 91 K with a very narrow transition ($\Delta T_c < 0.5$ K) and a mid-point at 91.5 K. The field sensitivity is also very weak. The critical current density deduced from magnetization studies [51] by the Bean model reaches 1.3×10^4 A cm^{-2} at 77 K and for 1 T ($H\|c$). Recent studies by dynamic hysteresis loops and magnetization relaxation have shown a clear correspondence between irreversible magnetization and pinning energies [52].

4. Discussion

Before going further in discussing the mechanisms implied in this kind of texturation, it is necessary to summarize our data. Increasing V_{max} is achieved by increasing T_{max} (here limited to 1170°C) and decreasing t_M and C_r. The quantities d_s and r_i decrease with increasing t_M and C_r; however, when t_M is too long, the sample gets heterogeneous. In the limit of 5°C/h, C_r is sufficiently slow to ensure a good peritectic recrystallization ($6 < d_s$ (%) < 30). The 211 mean particle size is remarkably insensitive to the thermal history (T_{max}, t_M, C_r). Indeed we did not observed a mean 211 particle size smaller than 5 μm or larger than 7 μm (see Tables 1 and 2); this is therefore probably inherent to the MTG method. Obviously other parameters characteristic of the thermal cycle should have important implications on the development of the texture such as C_d, T_1 and T_2.

We will now draw attention to the mechanisms implied in the 123 texturation, emphasizing the particular role of the Y_2O_3 substrate. We then discuss the

models proposed in the literature by comparing with our results.

4.1. 211 particle size

The mean 211 particle size is remarkably independent of the time t_M spent in the high-temperature step where the 211 grains are in contact with the liquid. Izumi et al. have made a similar finding [21]. During the solidification step, according to the theory of Uhlmann–Chalmers–Jackson [26], only particles larger than a critical radius can be trapped by the liquid/solid interface. Izumi et al. have shown that this theory applies to the peritectic recrystallization of 123; it is, however, difficult to give the critical radius precisely as no precise size-distribution measurement of 211 has been made up to now. However, the mean 211 particles size is in the range of 6 μm. The constancy of the 211 particles size in our samples proves that they should reach their final dimension very rapidly in the molten step. Coarsening by Ostwald ripening ($\alpha t^{1/3}$) which saturates rapidly with time is a possible mechanism. Izumi et al. came to the same conclusion; they also demonstrated [53] that very small 211 grains are obtained in QMG or MPMG methods due to the presence of platinum in the melt. The exact role of platinum is, however, still under discussion as it could also act as a nucleation modifier [54].

Together with the coarsening of the 211 particles, there is an opposite tendency for increasing T due to the phase diagram constitution. Upon increasing T above the peritectic temperature, the liquid is enriched in Y by an increasing dissolution of 211. Thus, there is a compromise between coarsening and dissolution of 211 particles leading rapidly to a pseudo-saturated radius as stated by Izumi et al. [21].

It should be recalled that as 211 particles are trapped in the crystallizing 123, the liquid is progressively enriched in copper (eventually up to the eutectic composition). Effectively, one finds in the solidified texture larger copper-rich inclusions either trapped in the texture or localized at the grain boundaries. Such areas are most of the time associated with interruption of the long-range order of the texture. This is certainly one of the limitations to reach large domain sizes. This underlines how important it is to activate Y supply to the liquid or to reduce 211 coarsening (by platinum refining) in order to decrease the residual 211 content (d_s, r_i) and particle size (l_m), a necessary path for long-range texturing.

4.2. On the Y dissolution in the peritectic liquid

It is now admitted that 211+L→123 peritectic crystallization is of the peritectic-reaction type as described in the introduction. This presupposes the system can reach a three-phase point where both primary solid (211) and 123 exist simultaneously with an undercooled Y enriched liquid according to m1. Many proofs of 211 dissolution in the liquid at or below the peritectic temperature can be found in the literature. By studying the effect of RE_2BaCuO_5 additions (RE=Sm, Y, Er) on 123 texturation, Balkin et al. [55] clearly show evidence of RE dissolution in the liquid. Rodriguez et al. [56] also established this phenomenon by in-situ observation of the high-temperature melting and solidification of 123 (high-temperature XRD, ESEM ...). According to their study, 211 grains act as an yttrium source and not as heterogeneous nucleation sites for the growth of 123. This implies that the secondary phase, i.e. 123, is grown by Y transport through the liquid. This is in agreement with recent experiments on laser zone melting proving the presence of a transformation zone, free of 211 according to electron microprobe analysis [57,58]. This zone is located close to the liquid/solid interface. In addition, one of us (Odier) has found that 123 crystals can be grown from Y_2O_3 or Y_2BaCuO_5 crucibles and BaO–CuO flux, initially free of Y [59]. In the first case, the crucible is rapidly covered with 211 which is textured and probably acts as nucleation sites for 123 [60]. The appearance of 123 in the solidified flux is a direct proof that 211 has been dissolved by the BaO–CuO melt. Moreover TEM observations on 123/211 interfaces in textured samples go in the same direction [49,34]. These results prove that Y dissolution occurs in the Y_2O_3–BaO–CuO liquid, but no quantitative data are known on the dissolution rate.

The 123 formation from the liquid is limited by several factors: the Y supply rate to the liquid, and overall chemical composition shifts due to losses of liquid by wetting or reaction with the substrate. Transport in the liquid is much faster than in the solid; Y solid-state diffusion in 211 should be therefore one

of the limiting steps of the process [61]. Losses of liquid are another obvious limiting factor. MgO single crystalline substrates are not wetted with the liquid, therefore not subject to such a problem. However, texturing with our procedure conducted on this substrate was inefficient in producing 123 textures totally free of 211, d_s remained in the range of $\sim 5\%$ with a mean 211 particle size ~ 5 μm [62]. We think this is a proof that one of the actual limitations is effectively Y solid-state diffusion in the 211 particles. An overall compositional shift is linked with the time spent at a high temperature. Decreasing T_1 is an efficient way to limit the interaction. Effectively we noticed a systematic tendency to form larger single domains upon decreasing T_1 below 1050°C. Surprisingly, one of the largest single domain obtained (≈ 100 mm^3) was formed in an experiment where the crystallization step was initiated at 1005°C, that is 10°C below the peritectic temperature. Certainly undercooling of the liquid plays an important role which is under investigation now.

4.3. Oriented 211 particles; consequences

The EPR study of textured domains demonstrates that there is a preferential orientation for a significant portion of the 211 inclusions in the 123 matrix. One can suppose this allows one to minimize the interfacial energy between 123 and 211 and thus to select the most appropriate orientation for the particle that is free to rotate in the liquid before being trapped in the solidification front. The result is a preferred occurrence of $\boldsymbol{b}_{211}$ to lie in the $(\boldsymbol{ab})_{123}$ planes. This is also consistent with TEM observations of 211 inclusions [50,49]. As a result it was realized that in several cases, 211 interfaces have a particular orientation relationship with the 123 matrix and therefore can be potentially active as nucleating sites. This implicity recognizes some anisotropy in the nucleation on 211 particles. In certain conditions, however, nucleation on the 211 sites may be enhanced with respect to normal conditions such as to compete with the progression of the texture initiated at the Y_2O_3 substrate interface where 211 seeds have been formed. This interference is suspected to have influence, in the absence of a thermal gradient, only for large cooling rates, i.e. above 2°C/h, when a high supersaturation and an increased nucleating rate at the 211 sites is expected. The long-range order characteristics of the texture cannot longer exist in these conditions. Indeed above 2°C/h, no large texture may be achieved while at 2°C/h the growth is possible but with many defects. This scenario gives some weight to heterogeneous nucleation phenomena on 211 particles. It is consistent with the growth model described by Alexander et al. [33,63] leading to the conclusion that 211 particles may act as nucleation centers when the growth front abuts a 211 particle. This nucleation may enable the 123 to growth along the **c** direction and the 211 particles to be bypassed further by the lateral growth. This may result in a gap on the other side of the 211 particle more or less filled with rejected liquid [63]. Our own TEM studies agree with these observations [34].

4.4. Crystallization front

As stated by Alexander et al. and confirmed by us [34] and others, the growth front is not continuous in the sample; it is more likely to be cellular or dendritic. As a matter of fact, localized heterogeneous areas are often noticed (see section 3.1.1.) as well as growth-induced defects separating 123 stacking platelets (this is developed in a forthcoming paper). The main reason is the restricted 211 dissolution during the peritectic reaction as stated before.

The actual process on the Y_2O_3 substrate is made under a residual thermal gradient which is very small (< 1°C/cm). The crystallization probably starts at the 211 layer created by interaction of the liquid with Y_2O_3. Apparently the orientation follows that of the 211 layer and we expect the solidification front to move from the 211 interphase towards the periphery of the cylinder. Effectively the most heterogeneous zones are always found at one extremity or at the periphery of the cylinder whereas the sample heart is generally uniformly textured.

5. Conclusion

Large 123 textured domains of good quality according to X-ray pole figures have been obtained using a Y_2O_3 substrate and without a thermal gradient. We have been able to texture centimetric domains. These samples present good superconducting prop-

erties: $J_c = 1.3 \times 10^4$ A cm^{-2} at 77 K for 1 T has been measured on the largest one. Slow cooling rates C_r are necessary to achieve large textured domains; typically C_r should be below 5°C/h for texturation to start. The largest domains are obtained for C_r smaller than 2°C/h and when the maximal temperature reached, i.e. T_{max}, is high but smaller <1170°C to avoid excessive liquid removing.

The substrate reacts with the peritectic liquid ml above 1050°C which causes the formation of a 211 layer. This layer is an essential ingredient of the texturation on an Y_2O_3 substrate without any applied thermal gradient. The observation that this layer is probably textured justifies to consider it as a seed for the 123 growth. Interestingly the texturing effect in these conditions has an efficiency comparable to that of a magnetic field or thermal gradient.

We confirm that the peritectic recrystallization of 123 does not proceed according to the classical peritectic transformation. Instead many arguments concur to prove the dissolution of Y in the liquid and the direct crystallization of 123 from it. Undercooling should play an important role that has still to be quantified.

The 211 remaining particle size seems to be dictated by their growth occurring in the liquid and their subsequent trapping in the solid which is controlled by the law derived by Uhlman–Chalmers and Jackson.

An EPR study shows a preferential, not random, 211 orientation with respect to the 123 matrix. This probably allows one to minimize their interfacial energy. This very peculiar property should be considered with respect to pinning phenomena in the textured materials. On the other hand it should have important consequences on the nucleation of the 123 phase. It opens the possibility that a secondary heterogeneous nucleation exists on well oriented 211 particles competing with the progression of the crystallization front.

The crystallization of 123 is cellular and the precise understanding of the crystallization process is essential to explain the complex defective structure of the textured 123. Characterization of the microstructures of these samples will be published in a next paper. One of the main difficulties for long-range texturing on an Y_2O_3 substrate is to avoid chemical shifts of the liquid due to chemical reaction with the substrate which a problem which is now being studied.

Acknowledgements

This work was supported by Alcatel-Alsthom Recherche (centre de Marcoussis France) cooperative program PIRMAT: "ARC Microstructure of High-T_c Superconductors", and CPR: "strong currents". We would like to thank M. Gervais, P. Dubots and G. Duperray for many stimulating discussions, and P. Germi, M. Pernet, N. Raimboux and J. Simonato for technical help.

References

[1] S. Jin, T.H. Tiefel, R. Sherwood, M. Davis, R. van Dover, G. Kammlott, R. Fastnacht and H. Keith, Appl. Phys. Lett. 52 (1988) 2074.
[2] D. Dimos and P. Chaudhari, Phys. Rev. Lett. 61 (1988) 219.
[3] S. Jin, R. Sherwood, E. Gyorgy, T. Tiefel, R. van Dover, S. Nakahara, L. Schneemeyer, R. Fastnacht and M. Davis, Appl. Phys. Lett. 54 (1989) 584.
[4] V. Selvamanickam and K. Salama, Appl. Phys. Lett. 57 (1990) 1575.
[5] D. Shi, M.M. Fang, J. Akujieze, M. Xu and J.G. Chen, Appl. Phys. Lett. 57 (1990) 2606.
[6] P. McGinn, N. Zhu, W. Chen, S. Sengupta and T. Li, Physica C 176 (1991) 203.
[7] L. Gao, R.L. Meng, Y.Y. Xue, P.H. Hor and C.W. Chu, Appl. Phys. Lett. 58 (1991) 92.
[8] M. Gervais, P. Odier and J.P. Coutures, Mater. Sci. Eng. B 8 (1991) 287.
[9] M. Murakami, S. Gotoh, H. Fujimoto, K. Yamaguchi, N. Koshizuka and S. Tanaka, Supercond. Sci. Technol. 4 (1991) S43.
[10] Y. Ishikawa, S. Kohayashi, S. Yoshizawa, K. Tenya and H. Miyajima, Physica C 185–189 (1991) 2375.
[11] M. Murakami, in: Studies of high-Temperature superconductors, vol. 9 ed. A.V. Narkilar (Nova, Commack), to be published.
[12] L. Zhan, P.-X. Zhang, P. Ji, K.-G. Wang, J.-R. Wang and X.-Z. Wu, Supercond. Sci. Technol. 3 (1990) 490.
[13] J.-R. Fang and S.-H. Hu, Cryogenics 30 (1990) 445.
[14] V. Selvamanickam, C. Partsinevelos, A.V. McGuire and K. Salama, Appl. Phys. Lett. 60 (1992) 3313.
[15] R.J. Pollard, D.G. McCartney, N. McN. Alford and T. Button, Supercond. Sci. Technol. 2 (1989) 169.
[16] P. de Rango, M.R. Lees, P. Lejay, A. Suplice, R. Tournier, M. Ingold, P. Germi and M. Pernet, Nature (London) 349 (1991) 770.

[17] M. Morita and S. Takebayashi, Proc. ISS'90, submitted.
[18] M.C. Flemings, Solidification Processing, McGraw-Hill series in Materials Science and Engineering (McGraw-Hill, New York, 1974).
[19] Y. Shiohara, M. Nakagawa, T. Suga, K. Ishige, T. Oyama, T. Izumi, S. Nagaya, M. Miyajima, I. Hirabayashi and S. Tanaka, Adv. in Superconductivity II, Proc. 2nd Int. Symp. Superconductor (ISS'89, 14–17 November 1989), eds. T. Ishiguro and K. Kajimura (Springer, Tokyo, 1990).
[20] M.J. Cima, X.P. Jiang, H.M. Chow, J.S. Haggerty, M.C. Flemings, H.D. Brody, R.A. Laudise and D.W. Johnson, J. Mater. Res. 5 (1990) 1834.
[21] T. Izumi and Y. Shiohara, J. Mater. Res. 7 (1992) 16.
[22] H.W. Kerr, J. Cisse and G.F. Bolling, Acta Metall. 22 (1974) 677.
[23] D.H. StJohn, Acta Metall. Mater. 38 (1990) 631.
[24] N.J. Barker and A. Hellawell, Met. Sci. 8 (1974) 353.
[25] H. Fredriksson and T. Nylen, Met. Sci. 16 (1982) 283.
[26] D.R. Uhlmann, B. Chalmers and K.A. Jackson, J. Appl. Phys. 35 (1964) 2986.
[27] C.A. Bateman, L. Zhang, H.M. Chan and M.P. Harmer, J. Am. Ceram. Soc. 75 (1992) 1281.
[28] P.J. McGinn, W. Chen, N. Zhu, C. Varanasi, L. Tan and D. Balkin, Physica C 183 (1991) 51.
[29] S. Jin, G.W. Kammlott, T.H. Tiefel, T.T. Kodas, T.L. Ward and D.M. Kroeger, Physica C 181 (1991) 57.
[30] S.-Y. Lee and J.-W. Ko, J.J. Appl. Phys. 30 (1991) 43.
[31] E. Sarath Kumar Menon and H.I. Aaronson, Acta Metall. 35 (1987) 549.
[32] G. Spanos and H.I. Aaronson, Scripta Metall. 22 (1988) 1537.
[33] K.B. Alexander, A. Goyal, D.M. Kroeger, V. Selvamanickam and K. Salama, Phys. Rev. B 45 (1992) 5622.
[34] J. Ayache, N. Pellerin and P. Odier, submitted to Physica C.
[35] J.M. Heintz, C. Magro, P. Dordor, D. Chateigner, P. Germi, M. Pernet, D. Machadjik and J.P. Bonnet, Cryogenics 33 (1993) 270.
[36] I. Monot, M. Lepropre, J. Provost, M. Hervieu, G. Desgardin and B. Raveau, Supercond. Sci. Technol. 5 (1992) 60.
[37] M. Kimura and M. Tanaka, Physica C 174 (1991) 263.
[38] D. Chateigner, P. Germi, M. Ingold and M. Pernet, Physica C 185–189 (1991) 2411.
[39] A. Douy and P. Odier, Mater. Res. Bull. 24 (1990) 1119.
[40] P. Regnier, R. Le Hazif and L. Chaffron, Proc. of the Int. Conf. on Modern Aspects of Superconductivity, Paris, 1989 (IITT-International) p. 133.
[41] N. Pellerin, M. Gervais and P. Odier, Mater. Res. Soc. Symp. Proc. 275 (1992) 537.
[42] N. Pellerin, G. Jouan and P. Odier, J. Mat. Res. 8 (1993) 18.
[43] C.L. Lin, L.P. Wang, J.J. Chu and P.T. Wu, Physica C 185–189 (1991) 1993.
[44] A. Catana, R.F. Broom, J.G. Bednorz, J. Mannhart and D.G. Schlom, Appl. Phys. Lett. 60 (1992) 1016.
[45] Hu, J. Mater. Res. 7 (1992) 808.
[46] F. Mehran, Phys. Rev. B 46 (1992) 5640.
[47] P. Simon, J.M. Bassat, S.B. Oseroff, Z. Fisk, S.W. Cheong, A. Wattiaux and S. Shultz, Phys. Rev. B 48 (1993) 4216.
[48] T. Kobayashi, H. Katsuda, K. Hayashi, M. Tokumoto and H. Ihara, J.J. Appl. Phys. 27 (1988) L670.
[49] J. Ayache, N. Pellerin and P. Odier, Proc. 3rd Ecer's Conf., Madrid 1993, to be published.
[50] T. Yamamoto, S.K. Chan, J.G. Lu, T.R.S. Prasanna and R.C. O'Handley, Phys. Rev. B 46 (1992) 8509.
[51] D. Delagnes, N. Pellerin, A.R. Fert, P. Odier, A. Mari, X. Bozec and J.P. Redoules, Physica C 211 (1993) 355.
[52] D. Delagnes, N. Pellerin, A.R. Fert and P. Odier, submitted to Physica C.
[53] T. Izumi, Y. Nakamura, T.H. Sung and Y. Shiohara, J. Mater. Res. 7 (1992) 801.
[54] J.H. Park, H.W. Kim and J.T. Song, J. Mater. Sci. materials in electronics 4 (1993) 77.
[55] D. Balkin, C. Varanasi, M. Black and P.J. McGinn, Proc. MRS, 27 April–1 May 1992, San Fransisco.
[56] M.A. Rodriguez, B.-J. Chen and R.L. Snyder, Physica C 195 (1992) 185.
[57] N. Pellerin, P. Odier and M. Gervais, J. Cryst. Growth 129 (1993) 21.
[58] N. Pellerin, C. Gendre and P. Odier, to be published.
[59] P. Odier, unpublished.
[60] K. Dembinski, M. Gervais, P. Odier and J.P. Coutures, J. Less-Common. Met. 164&164 (1990) 177.
[61] T. Izumi, Y. Nakamura and Y. Shiohara, J. Mater. Res. 7 (1992) 1621.
[62] N. Pellerin, P. Simon, P. Odier, D. Chateigner, P. Germi, M. Pernet and J.P. Bonnet, Proc. 4rd Int. Conf. ICMAS 1992 Paris, Series ed. A. Niku-Lari (IITT international) p. 99.
[63] A. Goyal, K.B. Alexander, D.M. Kroeger, P.D. Funkenbusch and S.J. Burns, Physica C 210 (1993) 197.